Soft Matter

PAPER

View Article Online
View Journal | View Issue

Cite this: *Soft Matter*, 2020, **16**, 7835

Micellar structure and transformations in sodium alkylbenzenesulfonate (NaLAS) aqueous solutions: effects of concentration, temperature, and salt†

Aysha S. Rafique,[a] Sepideh Khodaparast, ‡[a] Andreas S. Poulos,[a] William N. Sharratt,[a] Eric S. J. Robles[b] and João T. Cabral *[a]

We investigate the shape, dimensions, and transformation pathways of micelles of linear sodium alkylbenzenesulfonate (NaLAS), a common anionic surfactant, in aqueous solution. Employing Small Angle Neutron Scattering (SANS) and surface tensiometry, we quantify the effects of surfactant concentration (0.6–15 wt%), temperature (5–40 °C) and added salt (≤0.35 M Na_2SO_4). Spherical micelles form at low NaLAS (≤2.6 wt%) concentration in water, and become elongated with increasing concentration and decreasing temperature. Addition of salt reduces the critical micelle concentration (CMC) and thus promotes the formation of micelles. At fixed NaLAS concentration, salt addition causes spherical micelles to grow into cylindrical micelles, and then multilamellar vesicles (MLVs), which we examine by SANS and cryo-TEM. Above a threshold salt concentration, the MLVs reach diameters of 100 s of nm to few μm, eventually causing precipitation. While the salt concentrations associated with the micelle-to-cylinder transformation increase only slightly with temperature, those required for the cylinder-to-MLV transformation exhibit a pronounced, linear temperature dependence, which we examine in detail. Our study establishes a solution structure map for this model anionic surfactant in water, quantifying the combined roles of concentration, temperature and salt, at practically relevant conditions.

Received 26th May 2020,
Accepted 25th July 2020

DOI: 10.1039/d0sm00982b

rsc.li/soft-matter-journal

1 Introduction

Surfactants are key components in numerous global formulations industries including personal and home care, food, coatings, pharmaceuticals, and agri-chemicals.[1–7] Owing to their amphiphilic structure many surfactants have high solubility in water, exhibiting complex lyotropic behaviour above a critical concentration.[8–12] In dilute solutions (typically below 20–30 wt%), surfactants form globular or more elongated micelles with dimensions of a few nanometers, within an isotropic fluid.[13–15] The shape, size and structure of micelles at the nanoscale determine the physical properties and functionality of the surfactant solution.[16–18] At higher concentrations, ordered liquid crystalline phases, such as hexagonal, cubic and lamellar phases commonly form.[9,10] Understanding the phase boundaries of surfactant systems as a function of concentration, temperature, and the presence of other additives, is central to the design of formulated products, influencing their efficiency in application and environmental impact.

Sodium linear alkylbenzenesulfonate, NaLAS, is one of the most commonly used anionic surfactants in the world, employed extensively in detergent formulations.[19] It is itself composed of several compounds which differ in alkyl chain length and phenyl isomer whose distributions are depicted in Fig. 1a. In practical applications NaLAS is often found at concentrations below 30 wt% and in the micellar phase. However, structural analyses of this phase and the effect of environmental variations intrinsic to its use, such as dilution, temperature, and presence of electrolytes in water, are largely missing in the literature. Previous studies have reported the existence of mixed micellar (L_1) and lamellar phases (L_α) for concentrations above 30 wt% of NaLAS. At such concentrations, a temperature increase above 30 °C was observed to modify the bilayer spacing of the lamellar phase, resulting in lateral phase separation and coexistence of multiple lamellar phases. This has been associated with the presence of multiple isomers or due to the increased ionic strength and the resulting interactions between the headgroup and the counter-ion.[20–22] In general, higher temperatures were found to yield a larger bilayer *d*-spacing, and this effect was more pronounced at lower NaLAS concentrations.[21]

[a] *Department of Chemical Engineering, Imperial College London, London SW7 2AZ, UK. E-mail: j.cabral@imperial.ac.uk*
[b] *The Procter & Gamble Company, Newcastle Innovation Centre, Newcastle-Upon-Tyne, NE12 9TS, UK*

† Electronic supplementary information (ESI) available. See DOI: 10.1039/d0sm00982b

‡ Present address: School of Mechanical Engineering, University of Leeds, Leeds LS2 9JT, UK.

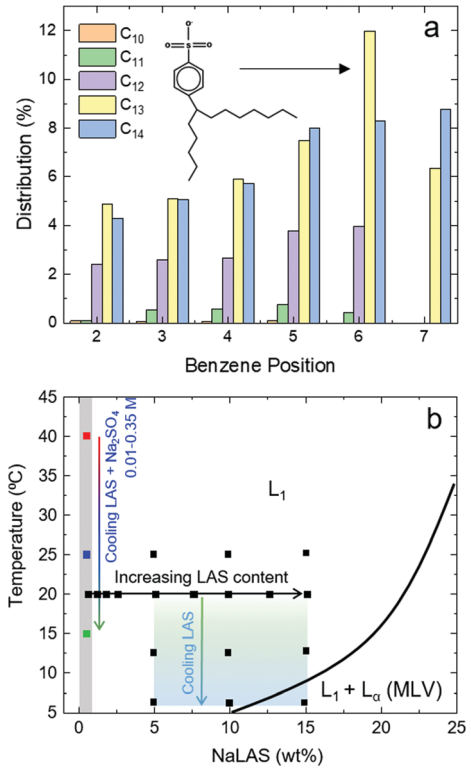

Fig. 1 (a) Distribution of phenyl positional isomers with different alkyl chain lengths in an industrial mixture of NaLAS. The chemical structure of the (most abundant) 6-phenyl isomer of NaLAS with a C_{13} chain is illustrated. (b) Phase diagram of NaLAS/H_2O (adapted from ref. 23), showing the regions corresponding to the micellar L_1 and the mixed $L_1 + L_\alpha$ (here MLVs) phases at relatively lower concentrations (<30 wt%). The filled black square markers indicate experimentally measured data for characterisation of effects of NaLAS concentration (0.5–15 wt%) and temperature (25 °C down to 6 °C) in binary NaLAS/water systems. The grey shaded area refers to measurements of selected ternary mixtures at 0.5 wt% NaLAS with varying amounts of added Na_2SO_4 salt (0.01–0.35 M) which were analysed at three distinct temperatures.

Below 30 wt%, the micellar phase of NaLAS has been reported to spontaneously transform into multilamellar vesicles (MLVs) upon cooling from room temperature (Fig. 1b).[23,24]

The effect of surfactant concentration on the shape and size of their micelles has been extensively reported for anionic, cationic and zwitterionic surfactants using small angle X-ray and neutron scattering techniques (SAXS and SANS).[25–27] Heating solutions of anionic sodium dodecyl sulfate (SDS) above room temperature was found to shrink ellipsoidal micelles.[26,28] Low-concentration surfactant solutions with longer alkyl chain lengths display large differences in viscosity over small increases in concentration that are often associated with changes of micellar structure from spherical to prolate ellipsoids and cylinders.[10] Interactions of surfactant molecules with soluble electrolytes in solution often occur as the result of either deliberate addition of salt in formulated products to achieve the desired functionality, or through the electrolytes already present in water. Generally, electrolyte ions reduce the repulsion between surfactant monomer ionic headgroups thereby making it more thermodynamically favourable to form micelles at lower surfactant concentrations.[29] The effect of electrolytes on the surface tension and critical micelle concentration (CMC) of surfactant solutions has been extensively reported over several decades;[10,30–32] salt addition typically reduces the surface tension of anionic surfactant solutions, with the effect becoming more pronounced at higher salt concentrations,[33–35] associated with the electrostatic interactions which promote the migration of surfactant monomers to the interface.[10,29,33,35,36]

The effect of added electrolytes on anionic micelles at surfactant concentrations above the CMC (in particular of SDS) has been extensively reported in terms of micelle shape, size, and thus functionality of the solution. The addition of sodium and lithium chloride were found to screen the intra- and inter-micelle repulsive forces, thus allowing the formation of larger aggregates.[37] SDS micelles have been shown to swell in the presence of other electrolytes.[38,39] Upon addition of sufficient salt, and often for multivalent ions common in 'hard' water (Ca^{2+}, Mg^{2+}), precipitation occurs. While significant effort has been dedicated to characterising the effect of electrolytes and temperature variations on the bulk properties of industrial surfactant solutions (*e.g.*, CMC, surface tension, detergency and solubility),[40,41] their impact on molecular-level structural transformations remains less understood.

In this paper, we seek to elucidate the effects of surfactant concentration, added salt and temperature – relevant to practical utilisation – on the shape, size and structure of NaLAS micelles in aqueous solution. Surface tensiometry is used to determine the CMC and establish the micellar region at varying salt concentration. We employ dynamic light scattering (DLS), SANS and cryogenic transmission electron microscopy (cryo-TEM) in the micellar phase to quantify effects of: (i) surfactant concentration (within a broad range 0.5–15 wt%), (ii) salt concentration (0.01–0.35 M of Na_2SO_4), and (iii) temperature variations above and below room temperature, as illustrated schematically in Fig. 1b. Our main goal is to identify and quantitatively characterise the pathways that lead to significant structural transformations within the micellar phase of NaLAS.

2 Materials and methods

A surfactant solution of 45 wt% NaLAS in water (H_2O), with isomer distribution shown in Fig. 1a, was obtained from Procter & Gamble and used as received. At this concentration and at room temperature the solution was heterogeneous, and it was thus heated at 65 °C for two hours and vigorously mixed to ensure its homogeneity before preparing the various solution series. Na_2SO_4 (99% purity) was purchased from Sigma Aldrich and used as received. Solutions were prepared by mass and stored at room temperature. Surface tension measurements and electron microscopy analyses were performed on solutions prepared by diluting the original NaLAS solution in DI water and stored at room temperature. To confirm sample homogeneity, surface tension and DLS measurements were carried out 3 times using freshly made solutions from the same batch source. For SANS measurements, the homogenised 45 wt%

NaLAS was further diluted in D_2O, thereby yielding NaLAS in isotopic water (H_2O/D_2O) mixtures of known ratio, relevant for background subtraction. Independent SANS measurements, performed on binary and ternary solutions of different NaLAS batches, show good agreement and corroborate the findings presented here (ESI,† Fig. S1 and S2).

2.1 Surface tension measurements

Surface tension measurements were carried out using the pendant drop method by Krüss EasyDrop Standard drop shape analysis system (DSA1). A series of NaLAS solutions ranging from 0 wt% to 2 wt% were prepared and made up to the desired concentration of Na_2SO_4. All samples were left overnight at room temperature prior to measurement. A drop of the filtered surfactant solution was dispensed under gravity using a blunt needle (d_i = 0.5 mm) and imaged optically. Experiments were repeated five times per sample, with ten surface tension measurements taken per droplet formed. The final surface tension measurement was reported as an average of all readings and with maximum estimated errors.

2.2 Dynamic light scattering

DLS measurements were performed on a Zetasizer Nano Z (Malvern Panalytical), equipped with a He–Ne laser of λ = 633 nm. A series of dilutions was made with varying concentrations of Na_2SO_4. Samples were filtered using a 0.2 μm syringe filter (ThermoFisher Scientific) before being loaded into a glass cuvette sealed with a screw cap (10 mm, Starna Scientific Ltd) to minimise evaporation, and allowed to thermally equilibrate at 25 °C for 5 min prior to data acquisition. Measurements were repeated three times using a fresh batch of dilutions from the stock NaLAS solution. Details of the estimation of hydrodynamic radii can be found in ESI,† Section S2.

2.3 Small angle neutron scattering

Solutions of NaLAS in H_2O/D_2O were prepared at different weight concentrations 0.6–15 wt% and SANS measurements were performed across a wide range of temperatures (5–25 °C). The effect of added salt was examined with solutions of 0.5 wt% NaLAS and 9 different concentrations of Na_2SO_4 (0–0.35 M), filtered using a 0.2 μm syringe filter (Thomas Scientific) and loaded into quartz cells (1 mm path length banjo, Starna); these measurements were carried out at 15, 25 and 40 °C. The range of NaLAS concentrations and temperatures covered in SANS experiments are illustrated in Fig. 1b. The measurements for NaLAS in water were performed at the D22 diffractometer (Institut Laue Langevin, Grenoble, France) using incident monochromatic λ = 6 Å and $\Delta\lambda/\lambda \simeq 10\%$ and those with added salt at varying temperature at LARMOR (ISIS, Didcot, UK) with a polychromatic λ = 0.9–13.3 Å beam with a sample-to-detector distance of 4.1 m. This yielded a range of $0.007 \leq Q \leq 0.5$ Å^{-1}. SANS data were reduced using GRASP and MANTID (for ILL and ISIS data, respectively)[42,43] by subtracting the scattering of the empty cell, and the correct H_2O/D_2O background, to yield the coherent scattering signal, and fitted with SASView.[44]

2.4 Cryo-TEM

A 3 μL droplet of sample solution was placed onto a copper TEM grid covered with a perforated carbon film in a controlled environment vitrifaction system (Vitrobot) at 25 °C and 95% humidity. The excess solution was removed *via* blotting with filter paper for 3 s. The sample was then placed into liquid ethane prior to storage in liquid nitrogen. The sample was examined with a Tecnai G2 Spirit Twin TEM at 120 kV and the images were captured using a CCD camera (FEI 2K Eagle Camera).

3 Results and discussion

We first report on the effects of surfactant concentration and temperature on the shape and dimensions of NaLAS micelles in water, based on SANS data from solutions above the CMC. We then focus on the effect of added salt on the formation of micelles, their shape, size, and finally the pathways of transformations from spherical micelles to elongated cylinders and eventually multilamellar vesicles.

3.1 Binary solutions of NaLAS/water

SANS experiments were carried out on solutions of NaLAS ranging from 0.6 to 15 wt%. Scattering Length Densities (SLD) of the sodium sulfonate shells ($\simeq$5 Å thickness) and carbon chain tails ($\simeq$13–15 Å length) were initialised at 1.69×10^{-6} Å^{-2} and -0.46×10^{-6} Å^{-2}, respectively, based on our previous work.[23] For clarity, details of SLD calculations and profiles are provided in ESI,† Section S3. No significant variation in the fitted SLD values were found upon increasing the concentration of NaLAS in binary mixtures, see ESI,† Fig. S5. Fig. 2a shows the SANS data and fits obtained with a core–shell prolate ellipsoidal model for the form factor $P(Q)$, and the Hayter–Penfold Rescaled Mean Spherical Approximation RMSA for the structure factor, $S(Q)$,[22,23,28,45] available in SASView.

Over the concentration range investigated, the scattering intensity curves of Fig. 2a exhibit a broad peak in the mid-Q region, characteristic of both inter- and intramicellar features of charged colloidal suspensions.[46,47] Upon increasing NaLAS concentration, the peak shifts towards higher Q and the shoulder appears steeper. The structure factor $S(Q)$ profile can be estimated from the coherent, calibrated scattering intensity as $S(Q) = I_{corr}(Q)/P(Q)$ (ESI,† Fig. S7), whose peak location Q_{peak} is shown in Fig. 2b, as a function of concentration. Two distinct trends are observed for concentrations below and above $\sim$5 wt% NaLAS, suggesting a change in micellar shape and size. In simple terms, assuming an ensemble of spherical micelles whose size remains constant and only the number density increases with volumetric concentration of surfactant C, the location of the peak at Q for each scattering profile would approximately follow $\log Q \propto \log C^{1/3}$. However, if micelles grow in size and also evolve in shape, a dependence $\log Q \propto \log C^{\alpha}$ where $\alpha < 1/3$ might be expected.[48] While Fig. 2b shows Q_{peak} obtained from $S(Q)$, ESI,† Fig. S7 also includes the peak location obtained from the total scattering intensity (and thus model-free), over the range of concentrations studied here.

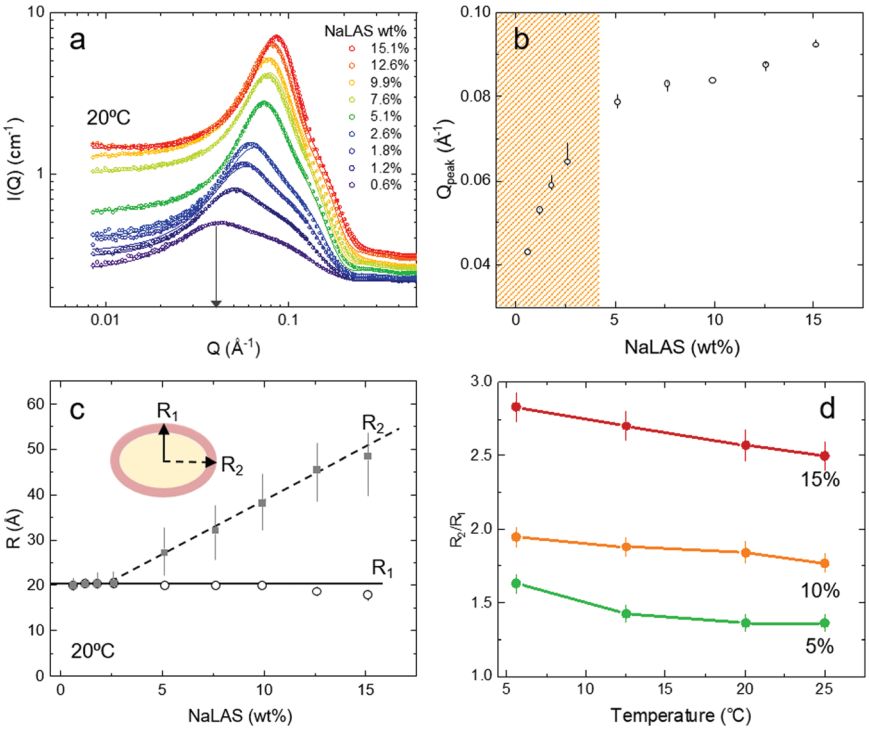

Fig. 2 SANS measurements of aqueous micellar solutions of NaLAS at different concentrations and temperatures. (a) Experimental SANS data (open circles) and the corresponding fitted model (solid lines) for increasing concentrations of aqueous NaLAS in water ranging from 0.6 wt% to 15.1 wt%. (b) Variation of the location of the peak Q_{peak} as a function of concentration of NaLAS wt%. Q_{peak} is obtained from plotting structure factor $S(Q)$ against Q (Å^{-1}) presented in ESI,† Fig. S7. Due to the change in the shape and size of the micelles two distinct regions were found for concentrations below and above 5 wt% of NaLAS. (c) For ellipsoidal micelles of NaLAS, the minor axis R_1 of the fitted ellipsoidal micelles remains unchanged, while the major axis R_2 elongates when increasing the concentration of NaLAS at a fixed temperature (here 20 °C). (d) The axial ratio of the micelles R_2/R_1 increases with decreasing temperature for different concentrations of NaLAS.

The trends are similar: for surfactant concentrations <5 wt%, $\alpha \approx 0.23$, while α decreases to ≈ 0.13 for higher concentrations, suggesting the formation of larger micelles yielding a smaller number density than expected for invariant micelle size.[49]

In line with the observations above, at low NaLAS concentrations (0.6–2.6 wt%) fits to the SANS measurements indicate the formation of near-spherical micelles with a ratio of major (R_2) and minor (R_1) axis of ellipsoids remaining close to unity ($R_2/R_1 \approx 1$), as shown in Fig. 2c. At NaLAS concentrations of 5 wt% and above, the major axis of the ellipsoidal micelles grows significantly, while the minor axis remains unchanged at about 20 Å in line with observations in other systems.[49,50] We find similar trends at different temperatures (Fig. 2d). In general, cooling below room temperature, caused further elongation of the prolate ellipsoidal micelles at fixed concentration, also in agreement with findings reported for other ionic surfactant micelles at relatively higher temperatures.[26,28]

3.2 Effect of added salt

3.2.1 Critical micelle concentration (CMC). We determined the CMC of the NaLAS sample to be 0.095 wt% in aqueous solution by surface tension γ measurements (Fig. 3a) using the point of intersection method (Fig. 3b), known to be reasonably accurate.[51] As shown in Fig. 1a, commercially available NaLAS contains several isomers and it has been previously shown[52–56]

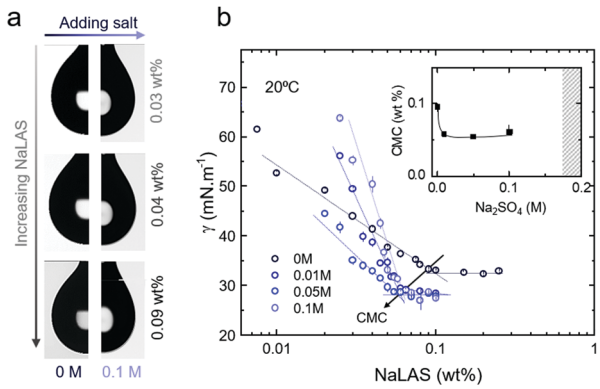

Fig. 3 Surface tension measurements of ternary NaLAS/water/Na_2SO_4 as a function of NaLAS concentration at room temperature. (a) Images of pendant drops of binary NaLAS/water (left) and ternary NaLAS/water/Na_2SO_4 (right) at different concentrations of NaLAS. Droplets are more elongated at higher surfactant concentration and added electrolyte due to the lower γ. (b) Surface tension of NaLAS solutions with and without added salt. The inset shows the evolution of CMC with increasing Na_2SO_4 concentration; the shaded area indicates salt concentrations tested where precipitation occurred.

that the position of the benzene group, the length of the alkyl chain and differences in molecular area can impact the slope of γ *vs.* concentration curve at lower concentrations, as well as the its value at CMC γ_{CMC}. A previous study[55] indicates that isomers

with headgroups positioned close to the centre of the alkyl chain tend towards higher γ and CMC values. These effects (and possibly dynamic adsorption) can account for the small variations in γ and data scatter in Fig. 3b.

The presence of Na_2SO_4 was found to reduce the CMC of NaLAS solutions, with the addition of 0.01 M salt yielding a CMC of 0.059 wt%, with no noticeable further change at higher salt (0.05 and 0.1 M), as shown in Fig. 3a and b. At even higher salt concentrations (>0.175 M Na_2SO_4), the solution was no longer homogeneous and the shaded region in the inset of Fig. 3b corresponds to where precipitation was observed optically (whose origin is discussed below). The value of γ also decreased, in general, with the presence of salt, with some scatter and deviations discussed above.

3.2.2 Micelles in ternary NaLAS/Na_2SO_4/water solutions. We next investigate the effect of electrolytes on NaLAS micelles (above the CMC values identified before) using SANS. Exploratory DLS experiments were used to estimate the hydrodynamic size of micelles in NaLAS/Na_2SO_4/water solutions, as shown in Fig. 4. DLS measurements were carried out on nine samples of 0.5 wt% NaLAS in solutions of different concentrations of Na_2SO_4. We observe that as the concentration of salt increases the time correlation function curves systematically move towards longer time scales indicating slower dynamics and larger micelles forming upon salt addition. A transition to much slower multi-component decay profiles is found for concentration of Na_2SO_4 (>0.2 M), in Fig. 4a.

A single exponential function can generally describe the time-dependent correlation data corresponding to the main population, with the exception of very low (0.01 M) and high salt concentrations (>0.2 M) where, respectively, data noise is greater or polydispersity is significant. Estimations of the apparent hydrodynamic radius R_h (since non-spherical micelles and vesicles can be expected) as a function of salt concentration are presented in Fig. 4b. Three regimes can be approximately identified, at fixed NaLAS concentration (0.5 wt% shown here): (i) for salt concentrations below 0.1 M, the estimated R_h increases slightly with added salt; (ii) for salt concentrations in the range of 0.1 M $\leq$ [Na_2SO_4] $\leq$ 0.2 M, R_h increases more steeply, while remaining <100 Å, and the solutions are optically clear; (iii) above 0.2 M of salt, R_h significantly increases to reach values of $\sim$200 Å and above, and a broad distribution of sizes is expected to exist; secondary DLS time decays appear (Fig. 4b) and then optically visible precipitation occurs in the solutions. Comparison of the current DLS findings and structural transformations reported in similar systems,[57–59] suggests that NaLAS micelles first elongate to form cylindrical structures before yielding larger assemblies such as multilamellar vesicles, previously reported for NaLAS solutions under other thermodynamic conditions[23] or external flow fields.[22] These postulated structures are illustrated in Fig. 4b, and are further examined by SANS in the following.

A concentration range of 0 M to 0.35 M Na_2SO_4 at fixed NaLAS concentration (here, 0.5 wt%) was investigated by SANS, and measurements started at 40 °C where all solutions are homogeneous and optically clear. Scattering profiles were then

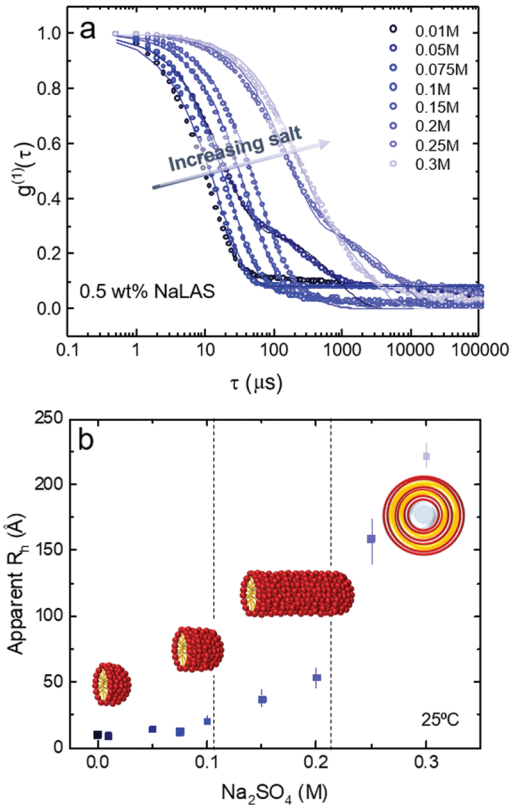

Fig. 4 Dynamic light scattering measurements of 0.5 wt% NaLAS solution with added electrolyte. (a) Experimental DLS data for 0.5 wt% aqueous NaLAS in compositions of increasing Na_2SO_4 concentrations ranging from 0.01 M to 0.3 M with fitted data superimposed. Upon the addition of salt, the curves systematically move towards the right side of the graph are associated with larger time scales. (b) Apparent hydrodynamic radius R_h as a function of Na_2SO_4 concentration.

also obtained at $T = 25$ °C and $T = 15$ °C to investigate the effect of cooling. Selected SANS data acquired at these three temperatures at different salt concentrations are presented in Fig. 5. Three distinct features can be observed in the SANS data upon increasing salt concentration across the different conditions: (i) Binary NaLAS/H_2O solutions yield an intermediate-Q peak arising from the electrostatic repulsive interaction of globular micelles. This intra-micellar repulsion appears to be screened at low salt concentration (0.1–0.15 M). (ii) An upturn in the low-Q region appears for the range of 0.1–0.2 M. (iii) The slope of the upturn in the low-Q region increases, while the micellar peak disappears, accompanied by the appearance of a high-Q Bragg peak. These qualitative findings are in general agreement with results of our DLS analyses. SANS data fitting quantitatively characterises the micellar structures and their transformations in these three different regimes.

3.2.3 Elongation of micelles. Micelles in binary 0.5 wt% NaLAS/water solutions are found to be spherical with core radius of about 15 Å and shell thickness of about 5 Å. Their electrostatic repulsive interaction yields a minimum in the low-Q region and a broad peak in the intermediate-Q region, depicted in Fig. 6a for 0 M salt concentration at $T = 25$ °C. Corresponding data for $T = 15$ °C and 40 °C are provided

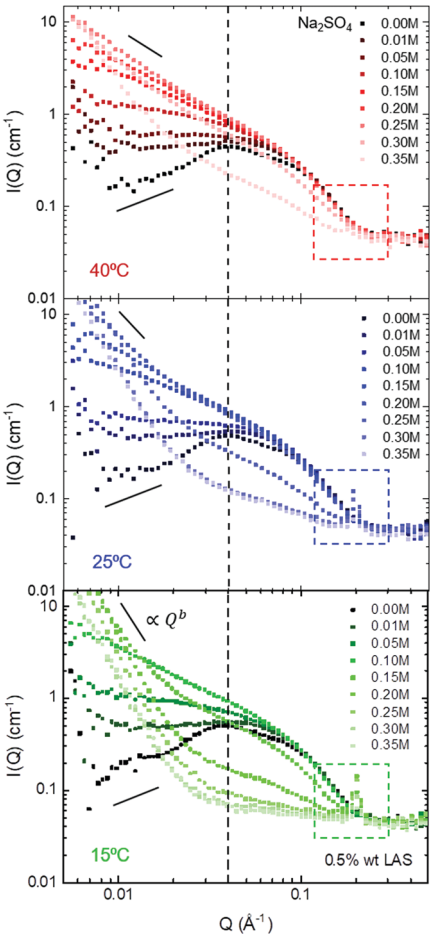

Fig. 5 SANS data for 0.5 wt% aqueous NaLAS mixed in a range of Na_2SO_4 concentrations (0 M to 0.35 M) upon cooling from 40 °C (top), 25 °C (middle), and 15 °C (bottom). The power law fits $I \propto Q^b$ to the scattering data in the low-Q range and the appearance of a Bragg peak in high-Q region (dashed square) are analysed in Sections 3.2.3 and 3.2.4, respectively.

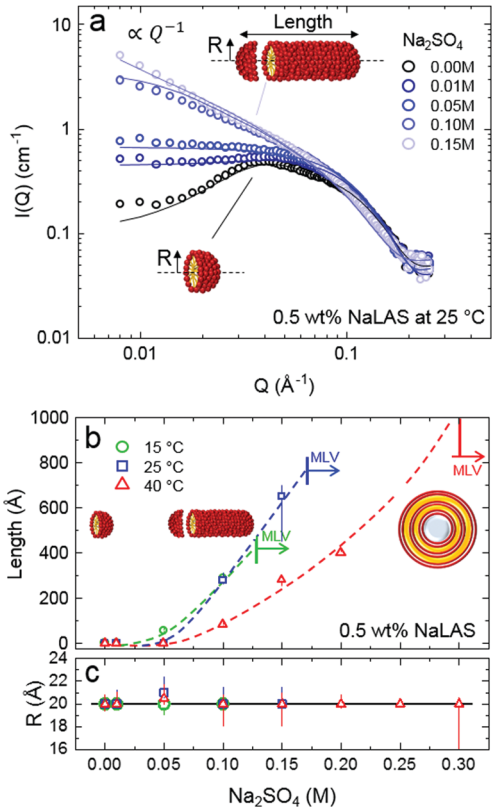

Fig. 6 Elongation of NaLAS micelles upon addition of salt as a function of temperature. (a) Experimental SANS data for 0.5 wt% aqueous NaLAS at 25 °C containing different Na_2SO_4 concentrations from 0 M to 0.15 M with fitted data superimposed. Data with peaks in the intermediate-Q region correspond to spherical micelles with radius R, while data with an upturn in the low-Q region are associated with solutions of cylindrical micelles of a similar radius. (b) Micellar length and (c) radius obtained by SANS data analysis. From initially spherical micelles (of similar dimensions with the temperature range investigated), added salt above ~0.05 M, causes cylindrical micelles to form, whose length increases with Na_2SO_4 concentration, in a more pronounced manner at the lower temperatures. Scattering data at higher salt concentrations, within the MLV regime, are not included here.

in ESI,† Fig. S9. The low-Q minimum disappears upon addition of 0.01–0.05 M of Na_2SO_4, associated with the screening of the negative charge of the micelles, thus reducing the repulsive interactions and flattening the SANS data in this Q-range. The manner in which sulfate ions affect the system has been investigated following the Hofmeister series, and shows that specific ion effects depend on salt concentration.[60,61] At low concentrations (<0.1 M) electrostatic forces dominate while at higher concentrations the electrostatic interactions are screened and so specific ion effects are likely more prevalent. The expected decrease of micellar charge upon addition of salt, obtained by SANS, is shown in ESI,† Fig. S10.

Adding salt in excess of 0.05 M salt to solutions of 0.5 wt% NaLAS, leads to a significant change in the form factor of the micelles. A power law fitted to the low-Q region indicates the formation of elongated micelles. Solutions of 0.1–0.15 M salt, were fitted using core–shell cylinder form factor. While the cylinder radius remains largely unchanged at around 20 Å, the length increases significantly at higher concentration of salt. A similar trend is observed at different temperatures where the transition from spherical micelles to cylinders occurs at lower salt concentration with decreasing temperature, see Fig. 6b. In this range, addition of salt to aqueous micellar solutions of NaLAS slightly modifies the SLD of the micellar shell and solvent as described quantitatively in the ESI,† Fig. S6.

Above a certain salt concentration, the slope in the low-Q region of SANS profiles significantly increases and cylindrical models can no longer describe the form factor. In this region, the sharp Bragg peak in the high-Q region indicates the formation of a multi-layer structure, likely attributed to the formation of multilamellar vesicles MLVs. While the transition from cylindrical to lamellar structures is found at all temperature investigated, the appearance of MLVs is observed at lower salt concentrations upon decreasing temperature, indicated by the vertical markers in Fig. 6b. Note that 0.3 M Na_2SO_4/NaLAS/H_2O solution at 40 °C contains cylinders that are longer than the measurement range accessible with the SANS diffractometer in this configuration $\left(L > \frac{2\pi}{Q_{\min}}\right)$. Conversely, higher

temperatures require a higher Na_2SO_4 concentration to trigger the phase change.

In general, the salt concentrations yielding the onset of transition from spherical to cylindrical, and cylindrical to MLVs, are in good agreement with of DLS measurements that suggested three distinct size ranges with added salt (Fig. 4b).

3.2.4 MLV formation and precipitation. SANS measurements at 15 °C reveal the presence of a Bragg peak at $Q \approx 0.2$ Å^{-1} in solutions above 0.10–0.15 M Na_2SO_4, and at higher salt concentration for higher temperatures. While the threshold salt concentration associated with the emergence of the peak depends on temperature, the peak position remains broadly constant within measurement variability (detailed in ESI,† Fig. S11a). An average *d*-spacing is calculated at 3.3 ± 0.3 nm, consistent with previous reports.[23,62] The peak intensity increases with added salt (above the required threshold value), corresponding to a higher volume fraction of lamellar phase, and then appears to decrease (ESI,† Fig. S11b). This, however, coincides with the onset of optical cloudiness (*e.g.*, ≃0.2 M Na_2SO_4 at 25 °C, and is reversible upon heating), which we attribute to the aggregation and sedimentation of larger MLVs, and is thus an apparent reduction of the peak intensity. Further increasing Na_2SO_4 concentration above this threshold was found to yield faster precipitation.

Upon sufficient salt addition (to a temperature-dependent threshold, see ESI,† Fig. S10), the headgroup repulsion between NaLAS monomers can be interpreted as sufficiently screened to enable closer packing[60,61] and greater counter-ion binding, often rationalised in terms of an increase in critical packing parameter (CPP) due to a 'reduction' in headgroup area. Overall these changes facilitate the adoption of a lamellar structure,[55,63] at specific salt-temperature conditions.

3.3 A temperature-salt morphology map

Previous studies have shown that analysis of the low-*Q* upturn can readily report on the structural characteristics of the solution.[64–66] Here, a $I \propto Q^b$ power law was fitted to the low-*Q* region to extract the relatively large-scale structural features of the solution. At all temperatures tested here, the *b* exponent systematically changes with increasing Na_2SO_4 concentration as shown in Fig. 7a: (i) at low salt concentrations, positive or zero *b*-values were obtained which are characteristic of spherical or ellipsoidal (globular) micelles. As the salt concentration increases *b* decreases indicating a structural transformation, (ii) first to $b \approx -1$, characteristic of a rod-like micelles, and then to (iii) an exponent closer to −3 to −4, indicative of aggregate behaviour or compact assemblies, such as vesicles. Stage (iii) is accompanied by the appearance of a Bragg peak in the high-*Q* region, associated with the lamellar *d*-spacing.

Fig. 7b describes the coupled effects of temperature and salt addition on the various structural transformations reported here. The addition of relatively small amounts of salt, screens the surfactant head-group repulsions and thus facilitates micellar packing and growth. As a general trend, as the temperature increases more salt is required to induce both transformations. However, the spherical-to-cylindrical transformation has only a slight positive temperature dependence, while the cylindrical-to-MLV transformation exhibits a stronger, linear dependence within the temperature range investigated. We associated this observation with an increase in solubility and additional thermal energy which disrupt ordering processes such as MLV formation.

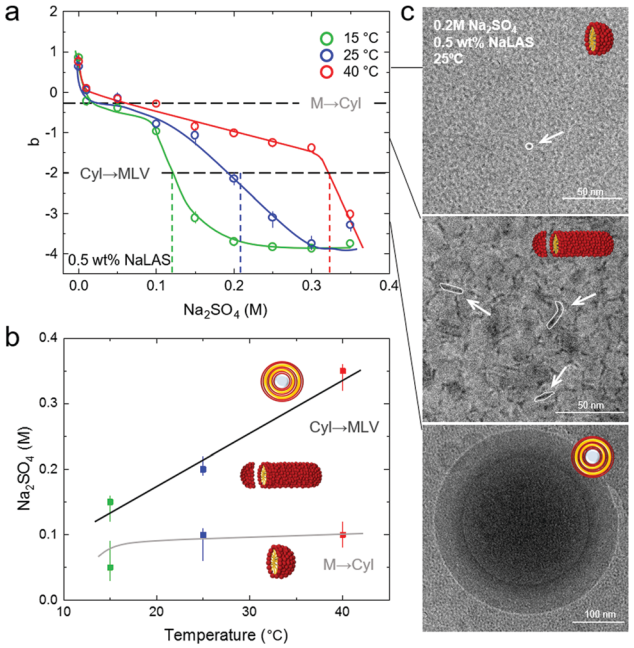

Fig. 7 Structural transformations in ternary NaLAS/Na_2SO_4/water solutions at low surfactant concentrations (here 0.5 wt%). (a) A power law, $I \propto Q^b$ was fitted to the SANS data in the low-*Q* range, and the *b* exponent is plotted as a function of Na_2SO_4 and employed as a facile means to classify the phase transformations from spherical/ellipsoidal to cylindrical micelles, to MLVs. Positive *b*-values arise from the structure factor contribution and are attributed to the electrostatic micellar repulsion, while negative values arise from the dominant form factor contribution. As the salt concentration increases the *b*-values change to −1 reflecting a cylindrical shape, eventually approaching $b \approx -4$ which is indicative of compact MLVs. (b) The Na_2SO_4 concentrations at which the shape transitions occur changes with temperature. At higher temperatures a more concentrated solution of salt is required. (c) Cryo-TEM images of 0.5 wt% NaLAS in 0.2 M Na_2SO_4 solution at 25 °C show the presence of micelles (top), cylindrical micelles (middle), and MLVs (bottom).

In order to visualise the different NaLAS aggregates in real space, we employ cryo-TEM and the images corroborate our DLS and SANS findings, see Fig. 7c (images with larger field of view are provided in ESI,† Fig. S12). Note that the small sampling volume, deposition on an external surface and the blotting procedure followed in our TEM analyses may lead to local variations of concentration and disturbance of structures due to inevitable mechanical stress. Therefore, TEM images are mainly provided as qualitative complementary data alongside the equilibrium bulk measurements obtained using DLS and SANS.

Several pathways for MLV formation from micelles have been proposed, including the formation of two-dimensional uni- or multi-layered disks from micelles, which then close and form vesicles upon reaching a maximum radius,[67–70] or the elongation of micelles to yield elongated, worm-like objects which coalesce and eventually create vesicles.[71,72] Our combined SANS and

cryo-TEM measurements show that MLVs in NaLAS/Na_2SO_4/water are generated through the latter mechanism, supported by evidence of micelle-to-cylinder, followed by cylinder-to-vesicle transformations.

4 Conclusions

NaLAS is one of the most widely used anionic surfactants in the world, in particular in laundry detergents, due to it biodegradable nature. Here, we have examined the solution phase behaviour of aqueous NaLAS as a function of: (i) surfactant concentration (ii) added salt, and (iii) temperature, within a range commonly found in practical applications, for instance in the context of detergents upon dilution, with varying temperature and water hardness. The parameter space investigated is relevant for the practical use of typical fabric liquid detergents and surface cleaners, with ramifications for cleaning efficiency, stability and optical appearance. We employed SANS to characterise the dependence of micellar structures and phase transformations across the parameter space, supported by pendant drop, DLS, cryo-TEM and optical measurements.

For NaLAS aqueous solutions, we observe spherical micelles with a radius of $\approx$20 Å at low surfactant concentrations ($\leq$2.5 wt%), beyond which the equatorial radius increases upon further NaLAS addition, resulting in ellipsoids with aspect ratio up to 3. Elongation is found to increase slightly ($\sim$10–15%) with decreasing temperature, from 25 to 5 °C. As expected, the presence of salt (Na_2SO_4) decreases the CMC of the surfactant solution, from $\simeq$0.095 wt% for NaLAS aqueous solution, to $\simeq$0.06 wt% which is nearly independent of salt content within 0.01–0.1 M; even higher salt concentrations cause precipitation of the solution. Alongside, the value of the surface tension at CMC drops from $\gamma_{CMC} \approx$ 33 to 28 mN m^{-1} upon salt addition.

Employing DLS, we find that the apparent hydrodynamic radius of NaLAS micelles increases pronouncedly with Na_2SO_4, suggesting the existence of micelle shape transformation at threshold salt concentrations, at a fixed temperature. Analysis of SANS data enables us to resolve three regimes in the solution structure, namely (a) near-spherical micelles, (b) formation of cylindrical micelles and (c) MLV formation, upon increasing salt content. The identification of micellar structures can be readily performed with SANS, from their characteristic low-Q power law exponents, as well as from the emergence of a lamellar peak upon MLV formation. The threshold salt concentration required to induce the transformation from spherical micelles to cylinders is found to be largely independent of temperature, at fixed surfactant concentration. The formation of MLVs, however, depends strongly on temperature, and lower salt concentrations are needed to promote cylinder-to-MLV transformation at lower temperatures, within the 15–40 °C range investigated. Cryo-TEM measurements corroborate our findings and provide real space insight into the overall solution structure, MLV size and polydispersity.

The average d-spacing of MLVs is estimated at 3.3 $\pm$ 0.3 nm, consistent with previously published data,[23,62] and varies relatively little with salt content and temperature, within measurement uncertainty. Above a sufficiently high salt content (*e.g.*, >0.2 M at 25 °C) surfactant precipitation takes place. As with the previous transformations, with increasing temperature, a higher salt content is required to induce precipitation.

In simple terms, aqueous NaLAS micellar solutions comprise spherical micelles or ellipsoids, upon increasing concentration. The addition of relatively small amounts of salt, screens the inter- and intra-micellar repulsion, thus facilitating packing and causing micelles to grow, first into cylinders ($\sim$0.1 M salt) and eventually into multilamellar vesicles, MLVs ($\sim$0.25 M). The salt threshold concentrations required to induce such changes increases with temperature, as added thermal energy disrupts these ordering processes. Overall, our study provides a comprehensive map and quantification of the micellar structure and transformations in solutions of NaLAS, a ubiquitous anionic surfactant, considering the coupled effects of surfactant concentration, added salt and temperature.

Conflicts of interest

There are no conflicts to declare.

Acknowledgements

We thank Procter & Gamble and the EPSRC-funded Advanced Characterisation of Materials CDT for a PhD scholarship for ASR. JTC acknowledges the Royal Academy of Engineering (UK) for a Research chair. We thank Robert Dalgliesh (ISIS) and Lionel Porcar (ILL) for assistance during SANS experiments and Paul A Simpson for help with cryo-TEM measurements. Experiments at the ISIS Neutron and Muon Source were supported by a beamtime allocation RB1820374[73] from the Science and Technology Facilities Council. This work benefited from the use of the SasView application, originally developed under NSF Award DMR-0520547. SasView also contains code developed with funding from the EU Horizon 2020 Programme under the SINE2020 Project Grant No. 654000.

Notes and references

1 G. J. Tiddy and A. Khan, *Curr. Opin. Colloid Interface Sci.*, 1999, **6**, 379–380.
2 J. Falbe, *Surfactants in consumer products*, Springer, 1987.
3 C. K. Ahn, Y. M. Kim, S. H. Woo and J. M. Park, *J. Hazard. Mater.*, 2008, **154**, 153–160.
4 J. J. Sheng, *Petroleum*, 2015, **1**, 97–105.
5 I. Kralova and J. Sjöblom, *J. Dispersion Sci. Technol.*, 2009, **30**, 1363–1383.
6 D. Myers, *Surfactant Science and Technology*, Wiley, 2005.
7 M. J. Castro, C. Ojeda and A. F. Cirelli, *Green Materials for Energy, Products and Depollution*, Springer, 2013, pp. 287–334.
8 S. Jain and F. S. Bates, *Science*, 2003, **300**, 460–464.
9 R. G. Laughlin, *The aqueous phase behavior of surfactants*, Academic Press, 1996.

10 B. Kronberg and B. Lindman, *Surfactants and polymers in aqueous solution*, John Wiley & Sons Ltd, Chichester, 2003.
11 T. F. Tadros, *Applied surfactants: principles and applications*, John Wiley & Sons, 2006.
12 B. Lindman and H. Wennerström, *Micelles*, Springer, 1980, pp. 1–83.
13 C. Tanford, *J. Phys. Chem.*, 1972, **76**, 3020–3024.
14 H. Wennerstrom and B. Lindman, *Phys. Rep.*, 1979, **52**, 1–86.
15 L. Maibaum, A. R. Dinner and D. Chandler, *J. Phys. Chem. B*, 2004, **108**, 6778–6781.
16 T. Shikata, H. Hirata and T. Kotaka, *Langmuir*, 1987, **3**, 1081–1086.
17 J. G. Weers, J. F. Rathman and D. R. Scheuing, *Colloid Polym. Sci.*, 1990, **268**, 832–846.
18 P. Kamranfar and M. Jamialahmadi, *J. Mol. Liq.*, 2014, **198**, 286–291.
19 I. Johansson and P. Somasundaran, *Handbook for cleaning/decontamination of surfaces*, Elsevier, 2007.
20 C. Richards, G. J. T. Tiddy and S. Casey, *Langmuir*, 2007, **23**, 467–474.
21 J. A. Stewart, A. Saiani, A. Bayly and G. J. T. Tiddy, *Colloids Surf., A*, 2009, **338**, 155–161.
22 A. S. Poulos, M. Nania, P. Lapham, R. M. Miller, A. J. Smith, H. Tantawy, J. Caragay, J. Gummel, O. Ces, E. S. J. Robles and J. T. Cabral, *Langmuir*, 2016, **32**, 5852–5861.
23 S. Khodaparast, W. Sharratt, H. Wang, E. S. Robles, R. Dalgliesh and J. T. Cabral, *J. Colloid Interface Sci.*, 2019, **546**, 221–230.
24 H. Wang, S. Khodaparast, J. Carroll, C. Kelly, E. S. J. Robles and J. T. Cabral, *Rev. Sci. Instrum.*, 2020, **91**, 045109.
25 D. Bendedouch, S. H. Chen and W. C. Koehler, *J. Phys. Chem.*, 1983, **87**, 153–159.
26 V. Y. Bezzobotnov, S. Borbely, L. Cser, B. Farago, I. A. Gladkih, Y. M. Ostanevich and S. Vass, *J. Phys. Chem.*, 1988, **92**, 5738–5743.
27 J. Gao, W. Ge and J. Li, *Sci. China, Ser. B: Chem.*, 2005, **48**, 470–475.
28 B. Hammouda, *J. Res. Natl. Inst. Stand. Technol.*, 2013, **118**, 151–167.
29 J. N. Israelachvili, *Intermolecular and surface forces*, Academic Press, 2015.
30 M. L. Corrin and W. D. Harkins, *J. Am. Chem. Soc.*, 1947, **69**, 683–688.
31 H. B. Klevens, *J. Phys. Colloid Chem.*, 1948, **52**, 130–148.
32 P. Becher, *J. Colloid Sci.*, 1962, **17**, 325–333.
33 S. Woolfrey, G. Banzon and M. Groves, *J. Colloid Interface Sci.*, 1986, **112**, 583–587.
34 S. S. Datwani and K. J. Stebe, *Langmuir*, 2001, **17**, 4287–4296.
35 M. Corrin and W. D. Harkins, *J. Am. Chem. Soc.*, 1947, **69**, 683–688.
36 C. Tanford, *The hydrophobic effect: formation of micelles and biological membranes*, J. Wiley, 2nd edn, 1980.
37 S. S. Berr and R. R. M. Jones, *Langmuir*, 1988, **4**, 1247–1251.
38 P. Debye and E. W. Anacker, *J. Phys. Chem.*, 1951, **55**, 644–655.
39 M. Almgren, J. Gimel, K. Wang, G. Karlsson, K. Edwards, W. Brown and K. Mortensen, *J. Colloid Interface Sci.*, 1998, **202**, 222–231.
40 L. Cohen, A. Moreno and J. L. Berna, *J. Am. Oil Chem. Soc.*, 1993, **70**, 79–82.
41 Y. Cao, R.-h. Zhao, L. Zhang, Z.-c. Xu, Z.-q. Jin, L. Luo, L. Zhang and S. Zhao, *Energy Fuels*, 2012, **26**, 2175–2181.
42 O. Arnold, J.-C. Bilheux, J. Borreguero, A. Buts, S. I. Campbell, L. Chapon, M. Doucet, N. Draper, R. F. Leal and M. Gigg, *et al.*, *Nucl. Instrum. Methods Phys. Res., Sect. A*, 2014, **764**, 156–166.
43 GRASP, https://www.ill.eu/en/users/support-labs-infrastructure/software-scientific-tools/grasp/, 2003.
44 SasView Project, http://www.sasview.org/, 2020.
45 J. Hayter and J. Hansen, *Mol. Phys.*, 1982, **46**, 651–656.
46 J. B. Hayter and J. Penfold, *Mol. Phys.*, 1981, **42**, 109–118.
47 T. Zemb and P. Charpin, *J. Phys.*, 1985, **46**, 249–256.
48 S. H. Chen, E. Y. Sheu, J. Kalus and H. Hoffman, *J. Appl. Crystallogr.*, 1988, **21**, 751–769.
49 V. Aswal and P. Goyal, *Chem. Phys. Lett.*, 2003, **368**, 59–65.
50 J. Iyer and D. Blankschtein, *J. Phys. Chem. B*, 2012, **116**, 6443–6454.
51 S.-Y. Lin, Y.-Y. Lin, E.-M. Chen, C.-T. Hsu and C.-C. Kwan, *Langmuir*, 1999, **15**, 4370–4376.
52 D. L. Smith, *J. Am. Oil Chem. Soc.*, 1997, **74**, 837–845.
53 Y. Zhu, M. J. Rosen, S. W. Morrall and J. Tolls, *J. Surfactants Deterg.*, 1998, **1**, 187–193.
54 V. Fainerman, E. Lucassen-Reynders and R. Miller, *Colloids Surf., A*, 1998, **143**, 141–165.
55 J.-G. Ma, B. J. Boyd and C. J. Drummond, *Langmuir*, 2006, **22**, 8646–8654.
56 R. Miller and G. Kretzschmar, *Adv. Colloid Interface Sci.*, 1991, **37**, 97–121.
57 K. D. Danov, P. A. Kralchevsky, S. D. Stoyanov, J. L. Cook, I. P. Stott and E. G. Pelan, *Adv. Colloid Interface Sci.*, 2018, **256**, 1–22.
58 D. Lombardo, M. A. Kiselev, S. Magazù and P. Calandra, *Adv. Condens. Matter Phys.*, 2015, **2015**, 151683.
59 P. Wang, S. Pei, M. Wang, Y. Yan, X. Sun and J. Zhang, *Phys. Chem. Chem. Phys.*, 2017, **19**, 4462–4468.
60 W. Kunz, *Curr. Opin. Colloid Interface Sci.*, 2010, **15**, 34–39.
61 W. Kunz, P. L. Nostro and B. W. Ninham, *Curr. Opin. Colloid Interface Sci.*, 2004, **9**, 1–18.
62 J. Stewart, A. Saiani, A. Bayly and G. Tiddy, *J. Dispersion Sci. Technol.*, 2011, **32**, 1700–1710.
63 A. Sein and J. B. Engberts, *Langmuir*, 1995, **11**, 455–465.
64 N. Jouault, R. Nguyen, M. Rawiso, N. Giuseppone and E. Buhler, *Soft Matter*, 2011, **7**, 4787–4800.
65 H. Frielinghaus, *Phys. Rev. E: Stat., Nonlinear, Soft Matter Phys.*, 2007, **76**, 051603.
66 J. E. Moore, T. M. McCoy, L. de Campo, A. V. Sokolova, C. J. Garvey, G. Pearson, B. L. Wilkinson and R. F. Tabor, *J. Colloid Interface Sci.*, 2018, **529**, 464–475.
67 J. Leng, S. U. Egelhaaf and M. E. Cates, *Biophys. J.*, 2003, **85**, 1624–1646.

68 K. Bressel, M. Muthig, S. Prevost, J. Gummel, T. Narayanan and M. Gradzielski, *ACS Nano*, 2012, **6**, 5858–5865.
69 T. M. Weiss, T. Narayanan, C. Wolf, M. Gradzielski, P. Panine, S. Finet and W. I. Helsby, *Phys. Rev. Lett.*, 2005, **94**, 038303.
70 C. Huang, D. Quinn, Y. Sadovsky, S. Suresh and K. J. Hsia, *Proc. Natl. Acad. Sci. U. S. A.*, 2017, **114**, 2910–2915.
71 M. J. Derry, O. O. Mykhaylyk and S. P. Armes, *Angew. Chem., Int. Ed.*, 2017, **56**, 1746–1750.
72 A. Blanazs, J. Madsen, G. Battaglia, A. J. Ryan and S. P. Armes, *J. Am. Chem. Soc.*, 2011, **133**, 16581–16587.
73 ISIS Neutron and Muon Source experiments RB1820374, DOI: 10.5286/ISIS.E.RB1820374.